Applied Geochemistry 100 (2019) 268–278

Contents lists available at ScienceDirect

Applied Geochemistry

journal homepage: www.elsevier.com/locate/apgeochem

Influence of iron on the alteration of the SON68 nuclear glass in the Callovo-Oxfordian groundwater

T. De Echave[a], M. Tribet[a,*], S. Gin[b], C. Jégou[a]

[a] CEA, DEN, DE2D, SEVT, LMPA, BP 17171, F-30207 Bagnols-sur-Cèze Cedex, France
[b] CEA, DEN, DE2D, SEVT, DIR, BP 17171, F-30207 Bagnols-sur-Cèze Cedex, France

ARTICLE INFO

Keywords:
SON68
Glass alteration
Iron
Corrosion

ABSTRACT

In France, the high level radioactive waste, contained in a glassy matrix, is intended for a deep geological disposal. It is then important to understand glass alteration, which depends on the near-field materials and the environmental conditions. The corrosion of the carbon steel overpack (used in the French multi-barrier concept for the disposal of high level radioactive waste) could influence glass alteration by the release of iron in the solution and the formation of iron corrosion products. For a better understanding of these interactions, different experiments were performed at 90 °C using a SON68 glass (non-radioactive surrogate of the R7T7 glass) separated by 80 µm from a pristine iron foil and immersed in synthetic groundwater. A pre-corroded iron foil and a PTFE foil, replacing the pristine iron foil, were also used. The influence of iron on glass alteration was studied, focusing on two different environments (the confined environment, inside the crack, and the diluted environment, where the faces are exposed to the homogeneous solution) and on the influence of a pre-corrosion of the iron foil. Depending on the previously described conditions, some variations were observed: as a whole, glass alteration increased in the presence of iron due to the precipitation of Fe-silicate minerals and it was also higher in the diluted environment than in the confined environment, indicating that the gel protective properties were different in both cases. This might be related either to differences in the solution composition in contact with the glass or differences in the gel composition, as it was shown that iron can enter the porous gel layer. In the tested conditions, pre-corrosion of an iron foil seemed to have no influence on glass alteration in a confined environment.

1. Introduction

In France, the confinement of radionuclides in a borosilicate glass matrix is the chosen method for disposal of high level radioactive waste. This solution is based on a multi-barrier concept: the glass incorporating in its structure the high level radioactive waste (fission products and minor actinides) is poured in a stainless steel canister which is contained in a carbon steel overpack of approximately 55 mm thick and is intended for disposal in the Callovo-Oxfordian (COx) claystone (ANDRA, 2005). Once the stainless steel canister is disposed in the geological repository, alteration is expected to occur mainly when water arrives in direct contact with the glass. This study focuses on this stage, which is expected to have the greatest impact on glass durability in the long term.

It has been reported that water will be in contact with the system after several hundreds to several thousand years, corroding the carbon steel overpack and altering the borosilicate glass (ANDRA, 2005). It has become a major scientific issue in radioactive waste management to understand the long-term evolution of glasses. It is then necessary to apprehend the interactions between glass, iron and the solution in order to assess and model the performance of this glass.

At first, the environment in the deep geological disposal will be aerated. Hence, the first stage of corrosion of the materials will take place in an aerated and dry environment. However, it has been predicted that the duration of this stage will last less than 100 years, oxygen will be actively consumed by corrosion of the materials and probably microbial activities, evolving from an anaerobic environment to an anoxic one (De Windt et al., 2014). When water is in contact with the system, the corrosion of the steel overpack in a reductive environment could lead to the precipitation of iron oxides and iron carbonates such as magnetite (Fe_3O_4), siderite ($FeCO_3$), chukanovite ($Fe_2CO_3(OH)_2$) with a considerable amount of iron released into the solution (Azoulay et al., 2013; Neff et al., 2005; Saheb et al., 2010).

Over the last decades, many studies have been performed to better

* Corresponding author.
E-mail address: magaly.tribet@cea.fr (M. Tribet).

https://doi.org/10.1016/j.apgeochem.2018.12.007
Received 22 February 2018; Received in revised form 5 December 2018; Accepted 5 December 2018
Available online 06 December 2018
0883-2927/

Table 1
Theoretical SON68 glass compositions in oxide weight percent.

Oxides	SiO_2	B_2O_3	Na_2O	Al_2O_3	CaO	ZnO	Li_2O	Fe_2O_3	P_2O_5	NiO
SON68	45.6	14.06	9.89	4.93	4.05	2.51	1.99	2.92	0.28	0.74
Oxides	Cr_2O_3	ZrO_2	Cs_2O	SrO	Y_2O_3	MoO_3	MnO_2	CoO	Ag_2O	CdO
SON68	0.51	2.66	1.42	0.33	0.2	1.71	0.72	0.12	0.03	0.03
Oxides	Sb_2O_3	SnO_2	TeO_2	BaO	La_2O_3	CeO_2	Pr_2O_3	Nd_2O_3		
SON68	0.01	0.02	0.23	0.6	0.9	0.93	0.44	2.13		

understand glass alteration and the fundamental mechanisms that control glass dissolution in pure water have been identified (Frankel et al., 2018; Frugier et al., 2008; Vienna et al., 2013). At first, glass dissolution starts with hydration and interdiffusion, which induces an ion exchange between protons in the solution and alkali in the glass. This process creates a hydrated glass layer that dissolves by hydrolysis of the silicate network. Then, the hydrolysis rate decreases due to the attainment of silicon saturation in the solution alongside the formation of a gel layer and secondary phases at the surface of the gel (Gin et al., 2011, 2017; Grambow, 1987; Van Iseghem et al., 2009). However, the relative importance of these various processes depends on several factors such as the water composition, water renewal, the near-field materials and the host rock.

When water is in direct contact with the glass, it will be at equilibrium with the near-field environment. This groundwater, rich in cations and anions that, could have an impact on glass alteration. It has been shown that in the hydrolysis process, some cations in the solution react with the glass surface creating Si—O-M sites (M represents the cations), weakening the Si—O bonds, which increases the hydrolysis rate and thus the alteration rate (Jollivet et al., 2012b). Moreover, while the gel grows, magnesium contained in the solution induces the formation of Mg-silicate minerals at the surface of the gel, which depletes the latter in silicon, a key network former; as a result, the glass dissolves faster (De Echave et al., 2018; Fleury et al., 2013; Jollivet et al., 2012a; Neeway et al., 2011). Most of the magnesium precipitates in secondary phases and once all consumed, the alteration rate can reach a value close to the one observed in deionized water (Rolland et al., 2012).

Furthermore, near-field materials, such as the claystone and the carbon steel overpack, seem to alter the mechanisms already established in deionized water (Dillmann et al., 2016; Neeway et al., 2015; Schlegel et al., 2016). Indeed, iron and its corrosion products tend to enhance glass alteration. Sorption of silicon on the iron corrosion products, such as magnetite, siderite and goethite, could be one cause of this increase (Godon et al., 2013; Jordan et al., 2007; Mayant et al., 2008; Michelin et al., 2013a). However, sorption phenomenon is limited over time by the saturation of the corrosion products surface sites (Philippini et al., 2006). Another explanation could be the precipitation of Fe-silicates at the surface of the gel (de Combarieu et al., 2011; Dillmann et al., 2016; Godon et al., 2013; McVay and Buckwalter, 1983). Unfortunately, there is only limited data in the literature concerning the nature of these secondary phases. Moreover, incorporation of iron into the gel layer has also been considered: it has been suggested that iron could be incorporated into the gel structure but most studies have shown that it precipitates in the gel porosity forming amorphous oxydrohydroxides or Fe-silicates (Dillmann et al., 2016; Michelin et al., 2013a, 2013b; Rull et al., 2004). Nevertheless, the current literature reveals some gaps in those mechanisms that need to be confirmed to better predict the long term behaviour of nuclear glass.

The aim of this study is to provide further information about glass alteration in the presence of metallic iron as a model system. The leaching experiments were then carried-out using a SON68 glass (non-radioactive surrogate of the R7T7 glass, the industrial French glass for high-level radioactive waste) separated by 80 µm from an iron foil (pristine or pre-corroded) in the synthetic Callovo-Oxfordian groundwater in an anoxic environment. This study allows us to compare the influence of iron on glass alteration in a confined environment (inside the crack) and in a diluted environment (where the faces are exposed to the homogeneous solution). Furthermore, information about the influence of an iron pre-corrosion on glass alteration is provided.

2. Materials and methods

2.1. Experimental setup

2.1.1. Glass sample

The SON68 glass was prepared by fusion of a mixture of oxides at 1150 °C for 3 h. Its composition is given in Table 1. The melted glass was then introduced into graphite crucibles of (2.5 × 2.5) cm^2 section and annealed for 2 h at 520 °C. A glass density of 2.75 ± 0.03 g cm^{-3} was obtained by hydrostatic weighing. The glass ingots were cut with a diamond saw into coupons of (2.5 × 2.5 x 0.2) cm^3. Each face of each coupon was polished to a glass surface roughness less than 1 µm, first with SiC papers and finally with a diamond suspension of 9 and 1 µm. The polished coupons were then cut in half with a dicing saw. All coupons were ultrasonically cleaned in acetone and then in absolute ethanol. The geometric surface area of each glass coupon was 6.8 ± 0.2 cm^2.

2.1.2. Leaching experiments

The experimental setup was composed of model crack samples leached at 90 °C in individual cells in the synthetic Callovo-Oxfordian clay-based groundwater solution (called then COx groundwater). The leaching solution was prepared from the COx groundwater composition at equilibrium with the clay rock calculated by the BRGM (French Geological Survey) (Gaucher et al., 2009). Its chemical composition is presented in Table 2. This solution was obtained by a mixture of different salts at different concentrations in deionized water. The pH was adjusted to a value of 6.36 at room temperature by CO_2 bubbling when all salts were dissolved. Then it was deaerated by a 3000 ppm CO_2 bubbling for 1 h to eliminate the oxygen dissolved in the solution.

Three series of model crack samples were made. They consisted of one SON68 glass monolith, measuring (2.5 × 1.2 x 0.1) cm^3 and one metallic iron foil of (2.5 × 1.2 x 0.0125) cm^3 (99.99% purity, Goodfellow) (Fig. 1). Two of the model cracks contained a pure iron foil and one sample contained a pre-corroded iron foil replacing the pure iron foil. The pre-corroded iron foil was obtained by introducing a pristine iron foil in the COx groundwater solution at 90 °C. After 30 days, the pre-corroded foil was extracted and used to prepare the glass-pre-corroded iron sample. Once the model crack assembled, the sample

Table 2
Theoretical chemical composition of the Callovo-Oxfordian clayey groundwater (mmol.L^{-1}) and pH measured at 20 °C.

Si	Na	K	Ca	Mg	Sr	Cl^-	SO_4^{2-}	HCO_3^-	$pH^{20°C}$
0.56	41.00	0.99	10.00	3.20	0.19	41.00	12.00	5.90	6.36

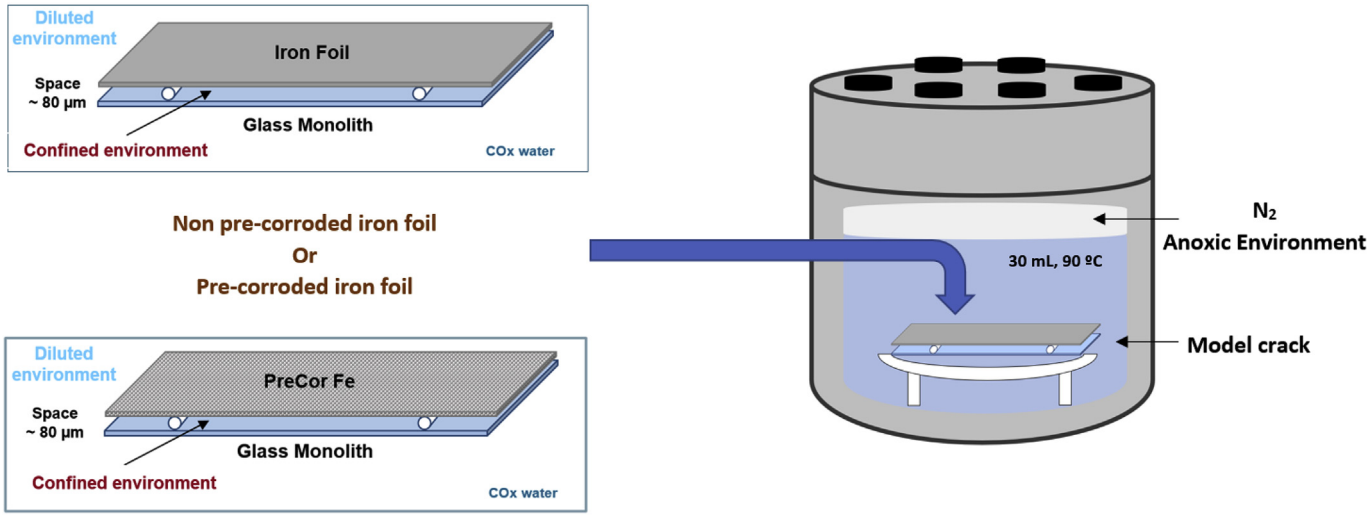

Fig. 1. Experimental setup: introduction of a model crack in a stainless-steel vessel with 30 mL of a COx groundwater solution and 10 mL of N_2 atmosphere. Leaching for 14 and 105 days at 90 °C. PreCor Fe stands for pre-corroded iron foil (30 days).

comprising a glass coupon and the pre-corroded iron foil was introduced in the same solution where the iron foil was pre-corroded. The model crack was then leached for 14 days.

A schematic view of the model crack is presented in Fig. 1 and its preparation is detailed as follows. The two materials were separated by two PTFE (PolyTetraFluoroEthylene) threads with a diameter of 80 µm. A small amount of high temperature RTV silicone instant gasket was introduced between both materials to ensure that they would stick together. This separation favors the interaction between both materials and was defined as the confined environment. The external sides open to the solution were defined as the diluted environment. In both cases, the model crack sample was introduced in a stainless-steel vessel, suspended in a Teflon basket and leached in 30 mL of the COx solution. All these leaching experiments were performed under anoxic conditions, in a glovebox under nitrogen atmosphere ($P(O_2) < 10$ ppm).

Samples were altered in the cells for 14 and 105 days when the pristine iron foil was used, and just for 14 days when the pre-corroded iron foil was used. A blank experiment was also carried out for 14 days where iron was replaced by a PTFE foil (inert material for glass alteration). At the end of each experiment, samples were extracted in the glovebox, dried at room temperature for 3 days and then embedded together with a very fluid epoxy resin (Buehler).

2.2. Analytical techniques

2.2.1. Leachate analysis

It was possible to have a first global result using solution analysis. The pH of the leachate was measured at the end of each experiment with an electrode AgCl calibrated at room temperature (buffer solution pH of 4 and 9) and with an uncertainty of ± 0.1. The leachate was analyzed by an ICP-AES Jobin Yvon JY66 system after acidification with ultra-pure grade HNO_3 at the beginning and the end of the experiment. Concentrations of Si, B, Li, Ca, Na, Fe and Mg were determined. The analytical uncertainty was ± 3%. Chlorides and sulfates were also analyzed with a Metrosep A Supp 16 ionic chromatography device to follow closely the concentrations of these elements. The analytical uncertainty was ± 10%.

2.2.2. Solid characterization

The pre-corroded iron foil was analyzed by micro-Raman spectroscopy using a Horiba Jobin-Yvon Xplora plus µ-Raman spectrometer coupled with a microscope. The excitation laser used was of 532 nm (green) focused on a (0.7 × 0.7) μm^2 spot and collected through a x100 objective. A laser power of 0.4 mW was used, low enough to avoid any iron oxidation (Neff, 2003).

The pristine iron foil was observed both directly and at the edge after embedding in the epoxy resin. All embedded samples were polished to a micron roughness and the surface of the polished cross sections were coated with carbon for observations and chemical analysis. Samples were first characterized by Scanning Electron Microscopy (SEM) coupled with an energy dispersive X-ray spectrometer device (EDS) with an environmental scanning electron microscope on a FEI Quanta 200 ESEM FEG microscope (partial pressure of 90 Pa, high tension between 3 and 15 kV) at the Marcoule Institute for Separative Chemistry (France). In this study it is assumed that glass alteration is an isovolumetric process, which means that the gel thickness equals the thickness of the altered glass. This is a reasonable assumption for this glass, as it was shown that even under aggressive conditions (e.g. glass in direct contact with clay) the gel thickness is a good proxy of the amount of altered glass (Gin et al., 2001).

Moreover, in order to study samples at the nanometer scale, a thin foil with a thickness of approximately 100 nm was prepared by the Focused-Ion Beam (FIB) technique with a dual-beam SEM/FIB microscope (LYRA GM TESCAN) at Tescan Analytics (Fuveau, France). Transmission Electron Microscopy (TEM) coupled with an energy dispersive X-ray Spectrometer Device (EDS) analysis was performed with a JEOL 2010F microscope at CP2M (Marseille, France) on the thin foil.

3. Results

3.1. Solution analysis

The solution was analyzed at the beginning and the end of the pre-corrosion of the iron foil and the model crack samples experiments (Table 3). These results represent only the bulk solution composition and do not give information about possible interactions in the confined environment between the glass and the iron foil nor exactly about the alteration in the diluted environment. At the end of the experiment, a solution sample was filtered at 0.45 µm and another sample was ultra-filtered at 10 000 Da in order to differentiate the colloidal material. In all experiments, results were the same, filtered or ultra-filtered, indicating that no colloidal material was formed.

After pre-corrosion of the iron foil, it was observed that the silicon concentration in the COx groundwater decreased as the iron concentration increased. However, Mg, Ca and Sr concentrations remained around the same value as the initial solution. It is important to highlight

Table 3
pH values and results by ICP-AES of the solutions composition before (initial solution) and after the experiments (mg.L^{-1}). GFeI stands for "glass-iron interaction", Bk for the glass-Teflon blank experiment, PreCor for pre-corroded iron foil.

Sample	Si	B	Li	Fe	Na	Ca	Mg	Sr	pH$^{20°C}$
Initial solution	15.5 ± 0.5	< 0.5	< 0.5	< 0.5	930 ± 28	389 ± 12	77 ± 2	16.2 ± 0.5	6.3 ± 0.1
PreCor 30 days	1.73 ± 0.2	< 0.5	< 0.5	5.8 ± 0.2	971 ± 29	330 ± 10	76 ± 2	14.9 ± 0.5	6.6 ± 0.1
GFeI-PreCor −14 days	9.1 ± 0.3	4.8 ± 0.1	1.8 ± 0.1	1.2 ± 0.1	1161 ± 35	400 ± 12	86 ± 3	17.7 ± 0.5	8.1 ± 0.1
Bk −14 days	24.0 ± 0.7	< 0.5	< 0.5	2.4 ± 0.1	1018 ± 31	411 ± 12	85 ± 2	17.1 ± 0.5	7.2 ± 0.1
GFeI – 14 days	3.5 ± 0.1	3.3 ± 0.1	1.6 ± 0.1	25.5 ± 0.8	1087 ± 33	367 ± 11	89 ± 3	15.4 ± 0.5	7.1 ± 0.1
GFeI – 105 days	2.5 ± 0.1	7.5 ± 0.2	2.5 ± 0.1	1.7 ± 0.1	1128 ± 34	373 ± 11	85 ± 3	15.2 ± 0.5	7.0 ± 0.1

that the pH value does not change significantly at the end of the iron pre-corrosion (from 6.3 to 6.6). When the cells were opened, it was possible to observe some precipitates in the solution, and some changes in the iron foil appearance, indicating that iron corrosion occurred.

Concerning the model cracks experiments, when glass and iron were both present in the system, B, Li and Na concentrations increased. Since these three elements are mobile and soluble elements from the glass and are used as glass alteration tracers, these results confirmed that glass was altered significantly under these conditions. Some variations were also observed in Si, Ca and Fe concentrations as well as an increase of pH values. The pH increase (around 0.8 pH unit) was the same when a Teflon foil, replacing the iron foil, was used. However, the pH value was higher when the iron foil was first pre-corroded (difference of 1 pH unit). In the blank experiment, which corresponds to a glass coupon altered in COx groundwater without an iron source, the concentrations of these tracers elements were under the detection limit (< 0.5 mg.L^{-1} for boron and lithium concentrations). This indicates that glass is more altered in the presence of iron. In the blank experiment, an increase in the silicon concentration was noticed contrary to the iron-bearing systems. Moreover, the pH value is the same as the one observed in the sample containing a pristine iron foil, the pH is then controlled by glass alteration. Unexpectedly, a small amount of iron was observed in the blank experiment. This is likely associated with an impurity in the stainless-steel vessel. Interestingly, magnesium concentrations had no significant variations, even if pH values were able to favor Mg-silicate precipitation under these conditions (pH > 6.5) (Jollivet et al., 2012a).

3.2. Solid characterizations

3.2.1. Pre-corrosion of the iron foil

SEM observations of the surface of the pre-corroded iron foil displayed 3 different phases (defined as cubes, sticks and sheets) and a corroded surface layer (Fig. 2). EDS analyses showed that the corroded surface layer contained mainly Fe, Si and O. The cubes contained a mixture of Fe, O and Ca, the sticks contained mainly Ca and O and the sheets contained mostly Si and Fe. EDS analysis on the polished cross section of the pre-corroded iron foil confirmed the surface analysis. Moreover, global observations of the cross section showed that the corrosion layer appears to be cracked (Fig. 2). This layer is inhomogeneous all along the iron foil. Using different images, a corrosion thickness of 16 ± 3 µm was determined. The pristine iron foil had an initial thickness of 125 ± 3 µm. After pre-corrosion, this value varied from 80 µm to 120 µm depending on the observed area.

Raman spectroscopy was also performed at different locations on the surface of the iron foil. It was possible to distinguish two different spectra: one from the sticks and another from the corroded surface layer (Fig. 2). It was not possible to use this technique to identify the sheets and cubes structures since it was difficult to differentiate them using the optical microscope. The corroded surface layer was identified as siderite. It was possible to obtain its Raman spectrum since it is stable under the laser power. The main bands match with published siderite bands (Hanesch, 2009): the 184, 287 and 731 cm^{-1} bands and the more intense at 1085 cm^{-1}, arising from the C—O bond. The stick phase was identified as aragonite, a calcium carbonate with an orthorhombic crystal system. The aragonite Raman spectrum is complex, and it has been published that it has 30 different bands with different intensities (De La Pierre et al., 2014). The Raman spectrum presented in here shows 13 of those bands: at 111, 178, 246, 258, 700, 703, 715, 852, 1462 and 1575 cm^{-1}, two intense bands at 151 and 204 cm^{-1} and the most intense band at 1080 cm^{-1}, arising from the C—O bond.

3.2.2. Glass alteration in the presence of iron

The glass coupons were altered in the presence of a pre-corroded iron foil for 14 days and in the presence of a pristine iron foil for 14 and 105 days in the same conditions. Results at the end of each experiment are presented as follows. A blank experiment, replacing iron by a Teflon foil was also performed. However, in this last case, SEM results are not presented in this paper since the alteration layer was too thin to be observed using this technique (glass alteration thickness < 300 nm). This result is in good agreement with the absence of glass tracer elements in the solution over the detection limit. It can thus be clearly assumed that glass alteration is higher when glass is altered in the presence of iron under the specific conditions of these leaching tests.

3.3. Impact of pre-corrosion of the iron foil

When the pre-corroded iron foil was used, it was possible to observe by SEM analysis an alteration layer on the glass phase and two different corrosion layers (corrosion products + secondary phases) on the iron foil. Some secondary phases were also observed (Fig. 3).

The alteration layer was highlighted using backscattering electrons due to its depletion in alkaline and alkaline earth elements. It was observed that at the edges, the glass alteration was larger. This could be due to a higher renewal of the solution at the edges increasing glass alteration (Chomat et al., 2012). These observations are in good agreement with results presented by Dillmann et al. using similar model cracks (Dillmann et al., 2016). In the confined environment, at the centre of the sample, it was possible to measure the thickness of the glass alteration layer using different images. All measurements were made using only SEM images. All results are summarized in Table 4. For the glass-pre-corroded iron foil sample, an average value of 1.3 ± 0.4 µm was obtained. However, in the diluted environment, the average value obtained was of 2.3 ± 0.3 µm. These different values could suggest that, in the confined environment, silica concentration in the solution was higher than in the diluted environment.

EDS results showed that the glass alteration was depleted in alkali, such as Na, and enriched with Fe. Moreover, some rare earth precipitates enriched in La and Nd were also observed all along the alteration layer. At the surface of the alteration layer, some secondary phases rich with Fe and Si were also observed.

On the iron phase, it was possible to observe by SEM analysis two different corrosion layers (Fig. 3). The layer next to the pristine iron foil was identified as the corroded layer formed during the pre-corrosion of the iron foil. It was rich with Ca and Fe and had some traces of Si. The second layer, closer to the glass, was defined as secondary phases which were also rich with Si, Ca and Fe. These phases, containing elements from the solution and the glass, were also formed at the surface of the

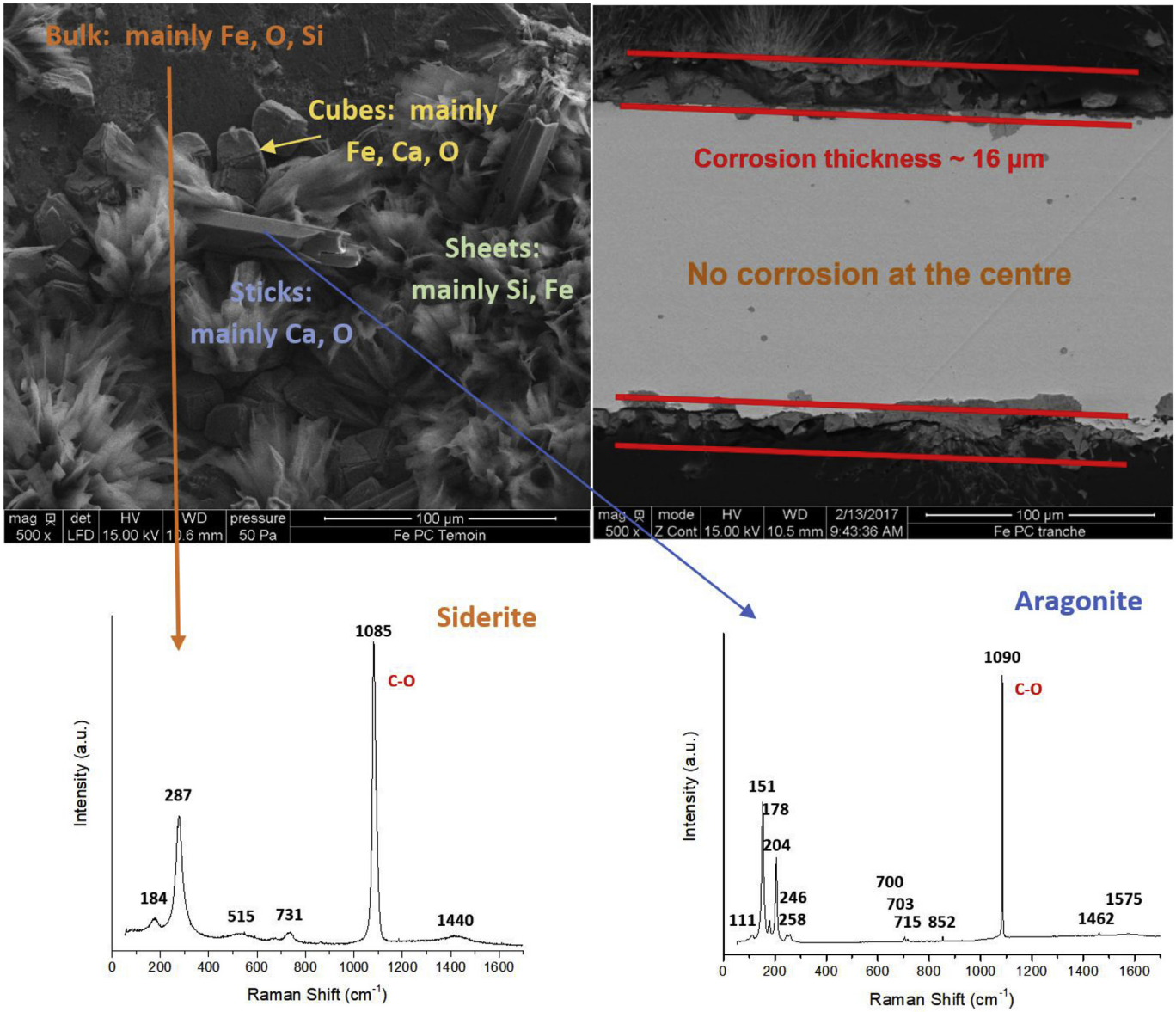

Fig. 2. SEM images of the surface of the pre-corroded iron foil (left) and a polished cross-section of the pre-corroded iron foil (right) after 30 days in COx groundwater (PreCor 30 days) and the Raman spectra of the phases observed at the surface of the pre-corroded iron foil containing mainly Ca and O and the corroded bulk.

glass. Furthermore, the iron surface exposed to the diluted environment was more corroded than the one exposed to the glass. Some precipitates, rich with Ca or Si and Fe, also reached the glass assuming that there could be a higher consumption of silicon in this area. However, no difference was observed in the glass alteration thickness when secondary phases reached the glass.

Using a pristine iron foil, after 14 days of leaching, SEM analysis showed similar results to the glass-pre-corroded iron sample (Fig. 3): a glass alteration layer and the formation of precipitates on the iron phase. However, only one corrosion layer was observed on the iron foil. Under these conditions, using different images, the thickness of the glass alteration layer in the confined environment at the centre of the sample was 1.3 ± 0.3 µm. This value is the same as the one observed when the pre-corroded iron foil was used. This could indicate that the pre-corrosion of the iron foil did not have an influence on glass alteration in the confined medium.

Moreover, the thickness of the glass alteration layer in the diluted environment was of 3.6 ± 0.5 µm, larger than the one formed when the pre-corroded iron foil was used. As seen in the previous case, when secondary phases, formed at the surface of the iron foil, reached the glass, no difference in glass alteration thickness was observed.

In conclusion, under these conditions, in the confined environment, there was no significant differences observed whether the iron source was pre-corroded or not. A small difference was observed in the diluted environment and it will be discussed in section 4.1.

3.4. Impact of leaching duration

Characterizations at the nanoscale on the altered glass of the 14 days glass-pristine iron foil sample were also performed. TEM observations showed that iron is present in all the alteration layer. However, its quantity decreased from the outer layer to the pristine glass (Fig. 4). The alteration layer was composed of two distinct areas. There was a first dense layer, next to the pristine glass, depleted in Na, Si and Al and enriched with Fe. Both its morphology and its composition suggest that this is the gel zone. There is also a second zone, containing sticks and sheets, rich with Si and Fe. This could be suggested as the secondary phases area which is formed at the surface of

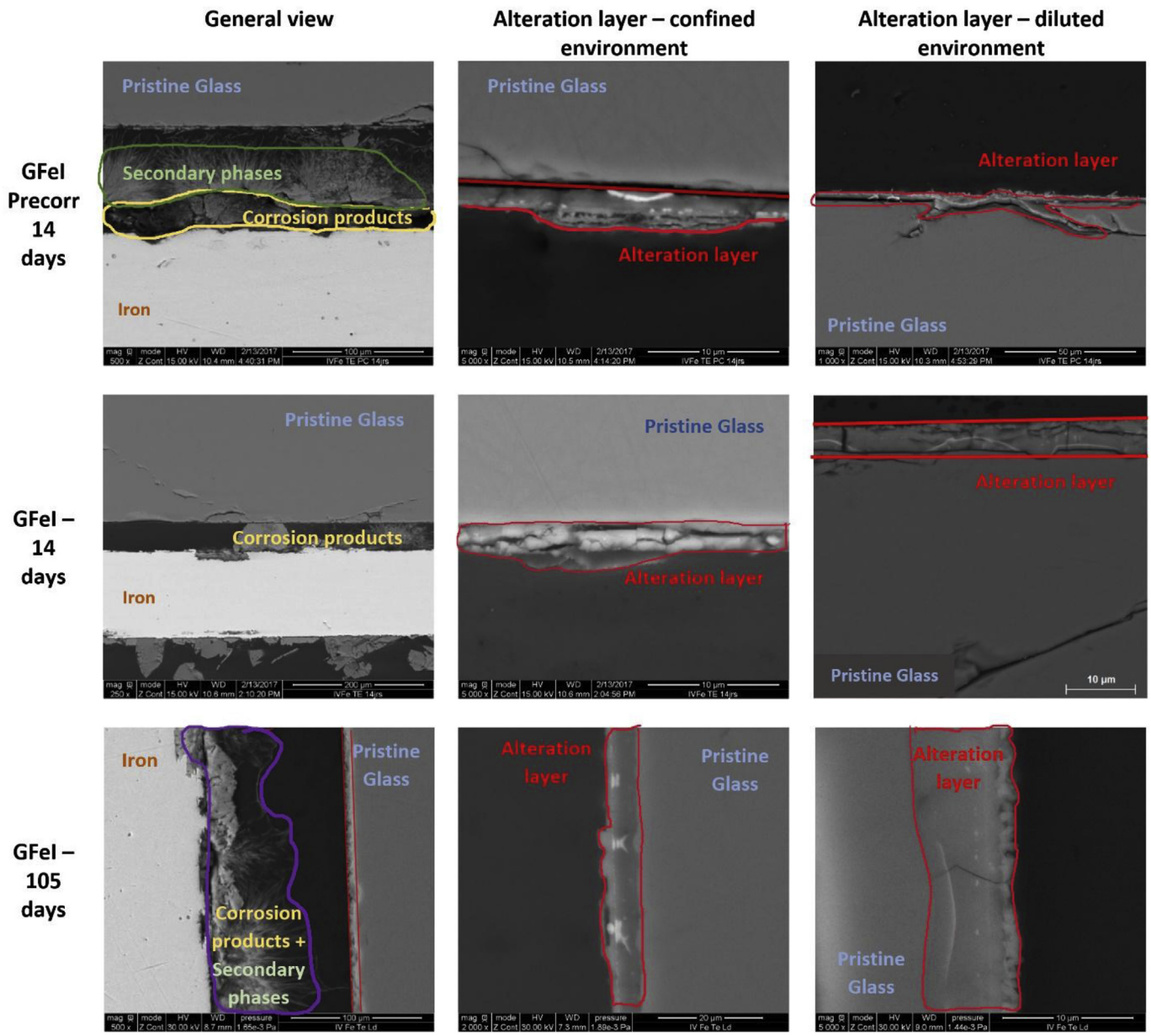

Fig. 3. SEM observations of the model crack experiments using a pristine iron foil (GFeI – 14 days) (GFeI – 105 days) and a pre-corroded iron foil (GFeI – PreCor- 14 days) after 14 days and 105 days of leaching. SEM images of a global observation of the model cracks, the glass alteration layer in the confined environment and the glass alteration in the diluted environment.

Table 4
Thickness of the glass alteration layer in the confined and in the diluted environment of all samples. GFeI stands for "Glass-iron interaction", Bk for the blank experiment, GFeI-PreCor for "Glass-pre-corroded iron foil".

Sample	Confined environment	Diluted environment
GFeI-PreCor 14 days	1.3 ± 0.4 µm	2.3 ± 0.3 µm
GFeI 14 days	1.3 ± 0.3 µm	3.6 ± 0.5 µm
GFeI 105 days	2.2 ± 0.4 µm	8.0 ± 0.7 µm

the gel. Moreover, EDS analysis also highlighted a thin layer at the surface of the gel enriched with Mg, indicating a possible incorporation of this element in the alteration layer or the formation of Mg−Si secondary phases.

Concerning the secondary phases, the sticks were rich with Fe and Si with some traces of Mg and with a Fe/Si ratio of 1.8. The sheets were also rich with Si and Fe but with some traces of Na, Mg, Ca, Mo and a Fe/Si ratio of 1.1. This could indicate the formation of two different Fe−Si secondary phases.

After 105 days of leaching, SEM analysis on the glass-pristine iron foil sample allowed the identification of the glass alteration thickness, in the confined environment, at the centre of the sample, of 2.2 ± 0.4 µm, thicker than the 14 days glass-pristine iron foil sample (Fig. 3 and Table 4). This means that even if a passivating layer was formed, the alteration of the glass increased versus time. In the diluted environment, the thickness of the glass alteration layer was of 8.0 ± 0.7 µm, twice larger that of the 14 days sample, also confirming that glass alteration increased versus time.

EDS results showed that there is also a significant amount of Fe incorporated in the alteration layer. As seen in the 14 days leaching experiment, the iron incorporation decreased from secondary phases to

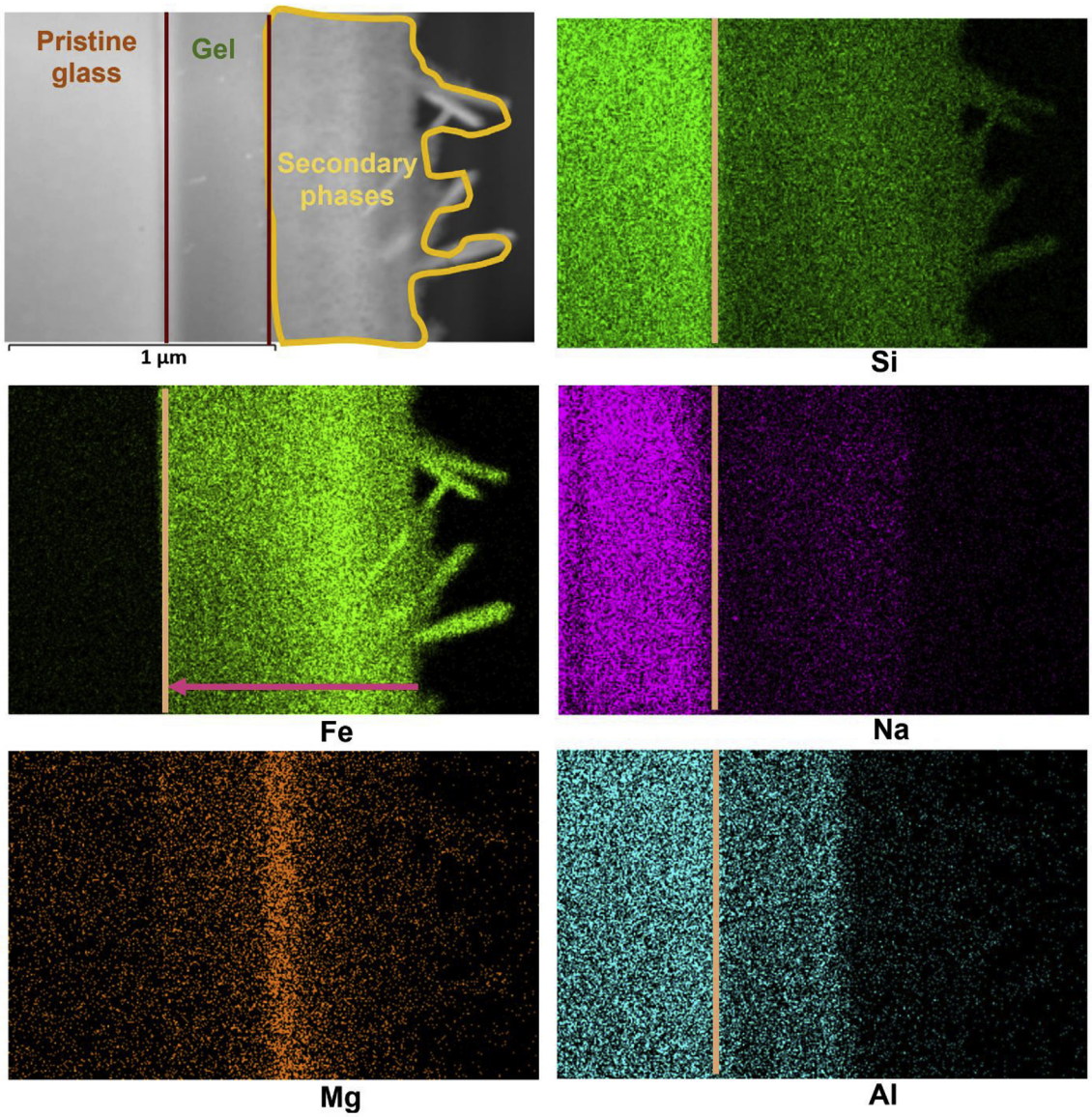

Fig. 4. TEM image and EDS analysis of the alteration layer of the SON68 glass in the confined environment after 14 days of leaching (GFeI – 14 days). The scale bar represents 1 µm.

the pristine glass. In the 105 days sample, no concentration of Mg at the surface of the gel was observed, as seen in the 14 days sample.

Under these conditions, the quantity and size of secondary phases were also higher than the 14 days sample: in the diluted environment as in the confined environment. Secondary phases were rich with Si and Fe, and some others rich with Ca. However, using only SEM images it was not possible to observe in the 105 days sample the two different morphologies of secondary phases observed by TEM analysis on the 14 days sample. Moreover, some rare earth precipitates were formed in the alteration layer. After 105 leaching days, these precipitates are larger than those observed in the 14 days sample.

4. Discussion

In our study, it was observed that glass alteration increases in the presence of an iron source. Comparing results after 14 days of leaching using a pristine iron foil or a pre-corroded iron foil, the glass alteration thickness was of approximately 1.3 µm in the confined environment for both experiments. However, in the diluted environment, the alteration thickness was different, of approximately 2.3 µm when a pre-corroded iron foil was used, and of approximately 3.6 µm when the pristine iron was used. Moreover, comparing results using only a pristine iron foil, it was observed that the glass alteration layer increased versus time. From 14 to 105 days of leaching, in the confined environment, it increases from 1.3 to 2.2 µm, while, in the diluted environment, it increases from 3.6 to 8 µm.

The increase of glass alteration in the presence of iron has already been reported in the literature and different mechanisms have been proposed to explain it (Godon et al., 2013; Michelin et al., 2013a): precipitation of Fe−Si secondary phases, incorporation of iron in the gel and sorption of silicon on iron corrosion products. Moreover, the use of a synthetic COx solution could also induce the precipitation of Mg−Si secondary phases, increasing also glass alteration (Debure et al., 2012, 2013; Fleury et al., 2013; Jollivet et al., 2012a). It has been proposed that a thicker glass alteration layer is formed when glass is leached in the presence of pure iron than in the presence of iron corrosion products (Rébiscoul et al., 2013; Michelin et al., 2013a). However, under the experimental conditions presented in our study, the use of a pre-corroded iron foil instead of a pristine iron foil gave no significant difference mostly in the confine environment. One may wonder the

reason for these similarities. Under the present experimental conditions, iron incorporation into the gel has been observed, but how does this incorporation take place in these systems? Furthermore, if iron is involved in the precipitation of Fe—Si secondary phases, what are these secondary phases? These different points will be discussed below.

4.1. Iron corrosion and its impact on glass alteration

Under the present experimental conditions in an anoxic environment, the main corrosion product obtained was siderite. This is in good agreement with data from the literature under similar experimental conditions (Neff et al., 2005; Romaine et al., 2013; Saheb et al., 2010). No other iron oxides nor iron carbonates were characterized in our system. However, in similar conditions, chukanovite could also precipitate (Michelin et al., 2015; Odorowski et al., 2017; Saheb et al., 2010). Moreover, under the experimental conditions presented in this paper, no calcite was observed as present in previous studies (Dillmann et al., 2016; Schlegel et al., 2014, 2016). Instead, aragonite was identified as the main calcium carbonate, with an orthorhombic crystal system (De La Pierre et al., 2014). Calcium carbonates can precipitate in different crystalline structures such as calcite, aragonite, vaterite. Aragonite can be formed at temperatures greater than 50 °C and seems to be more stable than others calcium carbonates (Wray and Daniels, 1957) which is in agreement with the present experimental conditions (90 °C). Our results are consistent with those obtained by a reactive-transport modelling of UOx pellets altered in the COx groundwater in the presence of iron (Odorowski et al., 2017). The model predicts a small local pH increase near the iron foil, favouring the precipitation of aragonite. Aragonite can also be favoured by the presence of significant concentrations of Mg^{2+}, ion present in the COx solution (Boyd et al., 2014; De Choudens-Sánchez and González, 2009).

The pre-corrosion of an iron foil for 30 days led to the formation of a large amount of corrosion products. Previous studies have shown that when only iron corrosion products are used, such as magnetite or siderite, the increase of glass alteration is less significant than when metallic iron is used (Michelin et al., 2013a; Rébiscoul et al., 2013). Therefore, according to the literature, in the confined environment, when the glass-pre-corroded iron model crack was used, glass alteration should have been controlled only by the iron corrosion products and it should have been lower than in the glass-pristine iron foil model crack. However, the thickness of the glass alteration layer was the same in both cases (approximately 1.3 μm). This strongly suggests that, in the systems presented here, iron continues to corrode and the availability of Fe in the solution was the same in both cases. Since the iron corrosion layer appeared to be cracked and inhomogeneous all along the surface of the pristine glass, it can be suggested that no protective layer at the surface of the iron foil was formed, or that the flux of Fe into the solution remained large enough and thus not rate-limiting.

In the literature, it has also been reported that when iron corrosion products such as magnetite or siderite are placed near the glass, sorption of silicon can take place with a limited impact (Godon et al., 2013; Michelin et al., 2013a; Neill et al., 2017; Philippini et al., 2006). This could have been observed in the glass-pre-corroded iron sample. However, it was not possible to observe any silicon sorption from the solid characterizations used in this study. This mechanism was certainly negligible compared to other mechanisms taking place at the time.

Furthermore, a difference between the thickness of the alteration layer in the diluted environment was observed: the alteration thickness was greater when a pristine iron foil was used than when a pre-corroded iron foil was used (2.3 μm compared to 3.5 μm after 14 leaching days). First, because these thicknesses are larger than the ones measured in the blank test, it can be concluded that iron affect glass alteration even though the source of iron is far from the glass. Second, regarding the difference noted above, it might be due to a pH effect. After 14 days of leaching, the bulk pH of the glass-pre-corroded iron sample was 8.1, contrary to the glass-pristine iron model crack sample, where the bulk pH was 7.1. In the literature, the pH influence on glass alteration depends on the regime studied. In the initial rate regime (controlled by the hydrolysis of the silicate network), glass dissolution increases when the pH increases, while the opposite effect is observed when a passivating gel is formed (rate drop and residual dissolution regime) (Gin and Mestre, 2001).

4.2. Glass alteration versus time

The glass alteration thickness of each sample was measured from different SEM images. If the glass was altered at its initial rate in the COx groundwater, the thickness of the altered glass can be calculated using the initial dissolution rate determined by Jollivet et al. of $r_0 = 1.7\ g\ m^{-2}.d^{-1}$ (Jollivet et al., 2012b). With such an alteration rate, after 14 days of leaching, these calculations lead to a glass alteration layer of approximately 9 μm, and after 105 days of leaching, of approximately 66 μm. Under the reasonable assumption that, under the tested conditions glass alteration is isovolumetric (alteration layer thickness = altered glass thickness), even when iron was present in the system and led to an increase of glass alteration, these alteration thicknesses were not reached. Thus, these results showed that glass alteration reached at least the “alteration rate drop” regime and are in good agreement with the formation of a protective gel layer.

In all samples, the thickness of the alteration layer was different in the confined environment and in the diluted environment. These observations could be related to the local solution characteristics. Within the model crack, the transport of water was likely controlled by diffusion meaning that the solution was poorly renewed (Chomat et al., 2012; Dillmann et al., 2016). In the diluted environment, no saturation of silica concentration was observed in the bulk solution, as it can be qualitatively observed from solution analysis (Table 3). Since the passivating properties of the gel mainly depend on the pH and on silica concentration, it can then be thought that there was a higher silica concentration in the solution at the centre of the crack, enabling the formation of a more passivating gel layer than in the diluted environment (Pèlegrin et al., 2010; Rebiscoul et al., 2005).

Furthermore, comparing the results of the glass alteration thickness after 14 days and 105 days of leaching, it is worth noting that the thickness of the glass alteration layer increased versus time in both environments (Fig. 5). Even though, in this study, it was possible to compare only two different leaching times, the glass alteration rate also decreased versus time: after a further 91 days of leaching, in both environments the glass alteration layer was only twice as thick. This suggests that, even with an unlimited iron source, a protective gel is formed decreasing glass alteration over time.

This effect could be explained by different hypothesis. First, it has been seen from solid characterizations, a significant iron incorporation into the glass alteration layer. If this incorporation contributes to the passivating properties of the gel, this mechanism could explain the decrease on glass alteration. Second, iron availability in the solution could have an important influence on glass alteration. On the one hand, if there is an overabundance of iron in the solution, the amount of silicon consumed by the precipitation of Fe—Si minerals could be sufficient to maintain the glass dissolution rate at its highest value (r_0). Nevertheless, this phenomenon has not been seen in our experiments. However, if the kinetics of precipitation of Fe—Si minerals is slow, even if both elements are in excess in the solution, a passivating gel could form and then glass alteration could decrease over time (kinetic limitation). On the other hand, if iron availability is limited in the solution, because it is controlled by the precipitation of corrosion product, then the consumption of this element will not lead to a total consumption of silicon in the solution and a passivating gel could also form (thermodynamic limitation). In both cases, the formation of a passivating gel leads to reach the rate drop regime. Unfortunately, the experiments presented in this study, do not allow to define which process was rate-limiting.

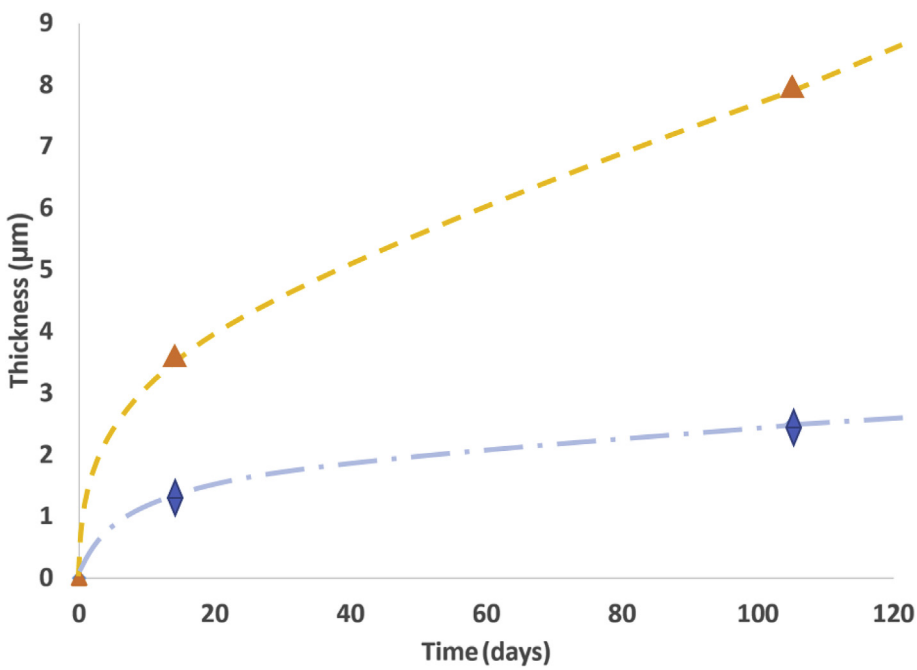

Fig. 5. Schematic view of the increase of the thickness of the glass alteration layer in the confined (centre of the model crack) in blue and in the diluted environment in orange versus time. The experimental data was obtained using different SEM images. Two data points were used for this figure and for each curve assuming a drop in the glass alteration rate and using the shape of the graph from (Vienna et al., 2013). (For interpretation of the references to colour in this figure legend, the reader is referred to the Web version of this article.)

4.3. Iron incorporation into the alteration layer

The passivating properties of the gel could be affected by the incorporation of iron or magnesium in the gel layer (Rebiscoul et al., 2004; Aréna et al., 2018). This incorporation could be explained as followed; precipitation of nanometric secondary phases in the gel pores or the incorporation of these two elements in the glass alteration layer as charge compensator for AlO_4^- and ZrO_6^{2-}, such as in the case of Ca (Chave et al., 2011; Mercado-Depierre et al., 2013; Thien et al., 2012). In a previous study, similar to the one presented in this paper, where two SON68 monoliths separated by an iron source were altered in the COx groundwater, it was observed that nanocrystals of greenalite precipitated in the gel (Dillmann et al., 2016). In another study, using a simple glass and with $FeCl_2$ constant additions in the solution, it has been proposed that there could be both, incorporation into the gel structure near the pristine glass, and precipitation of secondary phases in the gel pores, near the outer layer of secondary phases (Aréna et al., 2018). If there was an incorporation of Fe-silicates in the gel pores, a significant quantity of these secondary phases could "clog" these pores increasing the passivating properties of the gel (Jollivet et al., 2008; Michelin et al., 2013b). In our study, it was reported that the amount of iron decreased from secondary phases to the pristine glass: from approximately 15 mol.% in secondary phases to 9 mol.% in the gel and 0.7 mol.% in the pristine glass ($Fe_{nominal}$ = 0.8 mol.% in the pristine glass). There is no doubt that iron in the gel mostly came from the solution. The TEM data showed a regular decrease of iron concentration in the alteration layer. This could indicate that Fe—Si minerals precipitate within the pores formed by the release of mobile species and dissolved glass network formers. In fact, when glass is altered only in the COx groundwater, it has been observed that Mg—Si secondary phases form at the expense of the gel (De Echave et al., 2018). TEM observations showed that the porosity of the gel increases from the pristine glass to the secondary phases, indicating that the gel dissolves forming larger pores. This natural process has also been seen in the absence of the secondary phases (Ngo et al., 2018). In our study, the precipitation of Fe-silicates can be an additional driving force removing more matter from the gel. Since previous studies have observed greenalite in the gel (Dillmann et al., 2016), and since in our study the iron concentration in the gel decreases regularly from secondary phases to pristine glass, it can be suggested that in our cases, precipitation of Fe—Si secondary phases took place in the gel pores. This could explain why no empty pores have been observed in our study.

4.4. Precipitation of secondary phases

Previous studies have shown that glass alteration processes are mainly associated with the precipitation of secondary phases (Burger et al., 2013; Fleury et al., 2013; Inagaki et al., 1996; Jollivet et al., 2012a; Michelin et al., 2013b). In these conditions (COx groundwater + iron), precipitation of Fe-silicates or Mg-silicates is possible, which could lead to a significant silicon consumption, decreasing the gel passivating properties. It sustains glass dissolution and it can then be considered as a major driving force behind glass alteration. As suggested above, this detrimental effect might also be mitigated by the precipitation of Fe-silicates within the pores of the gel, potentially reducing the transport of reactive species between the glass surface and the bulk solution.

4.4.1. Fe-silicates

This phenomenon has been verified in the present systems: Fe-silicates were formed in every sample containing an iron source. These secondary phases were located mainly at the surface of the gel or near the iron corrosion products. In a recent study with a simplified glass, it has been suggested that the Fe-silicates formed are phyllosilicates belonging to the smectite group (Aréna et al., 2017; Burger et al., 2013; Schlegel et al., 2016). Moreover, another recent study using SON68 glass model cracks with an iron source incorporated in the aperture of the model crack, has shown that phyllosilicates, such as nontronite and greenalite, are formed at the surface of the gel, and in the gel pores (Dillmann et al., 2016). Under the experimental conditions presented here, from TEM-EDS analysis, it was not possible to identify these phases. However, two different structures of Fe-silicates at the surface of the gel were observed: one containing a Fe/Si ratio of 1.1 with a small concentration of Na and traces of Mg, Ca and another containing a Fe/Si ratio of 1.8 with traces of only Na, Mg. The different Fe/Si ratios and morphologies suggest thus that, under the present experimental conditions, two different Fe-silicates precipitated.

4.4.2. Mg-silicates

In previous studies, when there is a magnesium source, precipitation

of Mg-silicates has also been observed (Debure et al., 2012; Fleury et al., 2013; Jollivet et al., 2012a). There is a pH threshold value above which its precipitation is possible: at 90 °C it has been proposed to be at pH = 6.5 (Jollivet et al., 2012a). The pH values, obtained under the experimental conditions presented in this paper, were above the pH threshold value, enabling the precipitation of Mg-silicates. However, solution analysis results showed no significant consumption of magnesium. Moreover, it was observed that in the 105 days sample, using SEM-EDS analysis, no significant amount of magnesium was incorporated into the alteration layer. However, in the 14 days glass-iron foil sample, TEM-EDS analysis showed a small amount of Mg at the surface of the gel. In this case, its concentration was under 2 mol.%, indicating a very small Mg consumption. Even if pH conditions are favourable, Mg-silicate precipitation seems hampered by the formation of Fe-silicates. Geochemical modelling could help understand the reason, but thermodynamic properties of secondary phases are still missing to perform accurate calculations.

5. Concluding remarks

The aim of the present study was to investigate the SON68 glass alteration behaviour, in a synthetic groundwater, in the presence of an iron source under anoxic conditions. The influence of the iron source was studied using pure iron and a pre-corroded iron foil, and two different environments were also compared: a confined (inside the crack) and diluted (where the faces are exposed to the homogeneous solution) environment. All results are consistent between them.

Pre-corrosion of an iron foil led to a partial iron corrosion: a cracked and inhomogeneous corrosion layer was formed at the surface of the pristine iron. Iron corrosion led mainly to the precipitation of iron carbonates and calcium carbonates, where siderite and aragonite were identified. The pre-corrosion of the iron foil seemed to have no significant influence on glass alteration in the confined environment: there was the same iron availability in the solution in both systems (pre-corroded iron foil or pristine iron foil, leaching for 14 days).

In all conditions (iron pre-corrosion or not, alteration duration), a difference between both environments was also highlighted. In the diluted environment, glass alteration was greater than in the confined environment. It seemed that a more protective gel was formed in the confined environment than in the diluted environment indicating that glass alteration depended on local physico-chemical conditions. Moreover, it is worth noting that, in both environments, the glass alteration rate decreased versus time: the passivating properties of the gel increased then versus time.

This study confirms that glass alteration is greater in the presence of an iron source than without any iron source in both environments. The main processes observed in this study were the precipitation of Fe—Si secondary phases both on the surface of the gel and the iron foil and the incorporation of iron in the gel formed by glass alteration. The iron concentration in the gel diminished from secondary phases to the pristine glass suggesting that Fe—Si minerals precipitated within the porous gel. Secondary Fe-silicate phases were observed in all experiments containing an iron source. Two different Fe—Si phases were differentiated in terms of morphology and Si/Fe ratio but with the techniques used in this study, it was not possible to identify them.

In order to provide more data for modelling and to better understand the long-term behaviour of nuclear glass under disposal conditions, it is necessary to acquire more information about the nature, the crystallinity and the thermodynamic properties of the secondary phases which could form and affect the fate of silicon. Further experiments to measure the Fe(II)/Fe(III) ratio could then be performed in order to provide more information about the iron incorporation using EELS or STXM analysis (van Aken et al., 1998; Dillmann et al., 2016). Meanwhile, it is of primary importance to determine if the incorporation of Fe into the gel affects its passivation properties. This could be evaluated through isotopically spiked tracing experiments (Gin et al., 2015, 2017, 2018; Geisler et al., 2015; Lenting et al., 2018; Sessegolo et al., 2018).

The results presented in this paper allow us to have a first approach about the alteration of a SON68 glass separated by 80 µm from an iron source. However, since irradiation from radioactive waste contained in the glass could be an important factor in glass alteration, more experiments could be carried out using an α-doped SON68 glass (α-irradiation being predominant over time) in the same conditions as the experiments presented in this paper.

Acknowledgements

The authors are grateful to the CEA for their financial support. We would like to thank also Tescan Analytics (Fuveau, France) for the FIB cross section, and Martiane CABIE of CP2M (Marseille, France) for the TEM analysis.

References

ANDRA, 2005. Dossier 2005 : Argile, Évaluation de la faisabilité du stockage géologique en formation argileuse.
Aréna, H., Godon, N., Rebiscoul, D., Frugier, R., Podor, R., Garces, E., Cabie, M., Mestre, J.P., 2017. Impact of iron and magnesium on glass alteration: characterization of the secondary phases and determination of their solubility constants. Appl. Geochem. 82, 119–133.
Aréna, H., Godon, N., Rébiscoul, D., Podor, R., Garcès, E., Cabie, M., Mestre, J.P., 2018. Impact of Fe, Mg and Ca elements on glass alteration: interconnected processes. Geochim. Cosmochim. Acta. 239, 420–445.
Azoulay, I., Conforto, E., Refait, P., Rémazeilles, C., 2013. Study of ferrous corrosion products on iron archaeological objects by electron backscattered diffraction (EBSD). Appl. Phys. A 110, 379–388.
Boyd, V., Yoon, H., Zhang, C., Oostrom, M., Hess, N., Fouke, B., Valocchi, A.J., Werth, C.J., 2014. Influence of Mg2+ on CaCO3 precipitation during subsurface reactive transport in a homogeneous silicon-etched pore network. Geochem. Cosmochim. Acta 135, 321–335.
Burger, E., Rebiscoul, D., Bruguier, F., Jublot, M., Lartigue, J.E., Gin, S., 2013. Impact of iron on nuclear glass alteration in geological repository conditions: a multiscale approach. Appl. Geochem. 31, 159–170.
Chave, T., Frugier, P., Gin, S., Ayral, A., 2011. Glass-water interphase reactivity with calcium rich solutions. Geochem. Cosmochim. Acta 75, 4125–4139.
Chomat, L., Bouyer, F., Gin, S., Roux, S., 2012. Effect of leaching-driven flow on the alteration kinetics of an ideal crack in SON68 glass. J. Nucl. Mater. 426, 160–172.
de Combarieu, G., Schlegel, M.L., Neff, D., Foy, E., Vantelon, D., Barboux, P., Gin, S., 2011. Glass–iron–clay interactions in a radioactive waste geological disposal: an integrated laboratory-scale experiment. Appl. Geochem. 26, 65–79.
De Echave, T., Tribet, M., Jollivet, P., Marques, C., Gin, S., Jégou, C., 2018. Effect of clayey groundwater on the dissolution rate of SON68 simulated nuclear waste glass at 70 °C. J. Nucl. Mater. Submitted.
De Choudens-Sánchez, V., González, L., 2009. Calcite and aragonite precipitation under controlled instantaneous supersaturation: elucidating the role of CaCO3 saturation state and Mg/Ca ratio on calcium carbonate polymorphism. J. Sediment. Res. 79, 363–376.
De La Pierre, M., Carteret, C., Maschio, L., Andre, E., Orlando, R., Dovesi, R., 2014. The Raman spectrum of CaCO3 polymorphs calcite and aragonite: a combined experimental and computational study. J. Chem. Phys. 140.
De Windt, L., Marsal, F., Corvisier, J., Pellegrini, D., 2014. Modeling of oxygen gas diffusion and consumption during the oxic transient in a disposal cell of radioactive waste. Appl. Geochem. 41, 115–127.
Debure, M., Frugier, P., De Windt, L., Gin, S., 2012. Borosilicate glass alteration driven by magnesium carbonates. J. Nucl. Mater. 420, 347–361.
Debure, M., Frugier, P., De Windt, L., Gin, S., 2013. Dolomite effect on borosilicate glass alteration. Appl. Geochem. 33, 237–251.
Dillmann, P., Gin, S., Neff, D., Gentaz, L., Rebiscoul, D., 2016. Effect of natural and synthetic iron corrosion products on silicate glass alteration processes. Geochem. Cosmochim. Acta 172, 287–305.
Fleury, B., Godon, N., Ayral, A., Gin, S., 2013. SON68 glass dissolution driven by magnesium silicate precipitation. J. Nucl. Mater. 442, 17–28.
Frankel, G.S., Vienna, J.D., Lian, J., Scully, J.R., Gin, S., Ryan, J.V., Wang, J., Kim, S.H., Windl, W., Du, J., 2018. A comparative review of the aqueous corrosion of glasses, crystalline ceramics, and metals. npj Materials Degradation 2, 15.
Frugier, P., Gin, S., Minet, Y., Chave, T., Bonin, B., Godon, N., Lartigue, J.E., Jollivet, P., Ayral, A., De Windt, L., Santarini, G., 2008. SON68 nuclear glass dissolution kinetics: current state of knowledge and basis of the new GRAAL model. J. Nucl. Mater. 380, 8–21.
Gaucher, E.C., Tournassat, C., Pearson, F.J., Blanc, P., Crouzet, C., Lerouge, C., Altmann, S., 2009. A robust model for pore-water chemistry of clayrock. Geochem. Cosmochim. Acta 73, 6470–6487.
Geisler, T., Nagel, T., Kilburn, M.R., Janssen, A., Icenhower, J.P., Fonseca, R.O.C., Grange, M., Nemchin, A.A., 2015. The mechanism of borosilicate glass corrosion revisited. Geochem. Cosmochim. Acta 158, 112–129.
Gin, S., Jollivet, P., Mestre, J.P., Jullien, M., Pozo, C., 2001. French SON 68 nuclear glass

alteration mechanisms on contact with clay media. Appl. Geochem. 16, 861–881.
Gin, S., Collin, M., Jollivet, P., Fournier, M., Minet, Y., Dupuy, L., Mahadevan, T., Kerisit, S., Du, J.C., 2018. Dynamics of self-reorganization explains passivation of silicate glasses. Nat. Commun. 9, 9.
Gin, S., Guittonneau, C., Godon, N., Neff, D., Rebiscoul, D., Cabie, M., Mostefaoui, S., 2011. Nuclear glass durability: new insight into alteration layer properties. J. Phys. Chem. C 115, 18696–18706.
Gin, S., Jollivet, P., Fournier, M., Angeli, F., Frugier, P., Charpentier, T., 2015. Origin and consequences of silicate glass passivation by surface layers. Nat. Commun. 6.
Gin, S., Jollivet, P., Rossa, G.B., Tribet, M., Mougnaud, S., Collin, M., Fournier, M., Cadel, E., Cabie, M., Dupuy, L., 2017. Atom-Probe Tomography, TEM and ToF-SIMS study of borosilicate glass alteration rim: a multiscale approach to investigating rate-limiting mechanisms. Geochem. Cosmochim. Acta 202, 57–76.
Gin, S., Mestre, J.P., 2001. SON 68 nuclear glass alteration kinetics between pH 7 and pH 11.5. J. Nucl. Mater. 295, 83–96.
Godon, N., Gin, S., Rebiscoul, D., Frugier, P., 2013. SON68 glass alteration enhanced by magnetite. Procedia Earth and Planetary Science 7, 300–303.
Grambow, B., 1987. Nuclear Waste glass dissolution: mechanism, model and application. In: JSS-Projecy (Ed.), Report to the JSS-project Phase IV.
Hanesch, M., 2009. Raman spectroscopy of iron oxides and (oxy)hydroxides at low laser power and possible applications in environmental magnetic studies. Geophys. J. Int. 177, 941–948.
Inagaki, Y., Ogata, A., Furuya, H., Idemitsu, K., Banba, T., Maeda, T., 1996. Effects of redox condition on waste glass corrosion in the presence of magnetite. In: Murphy, W.M., Knecht, D.A. (Eds.), Scientific Basis for Nuclear Waste Management Xix, pp. 257–264.
Jollivet, P., Angeli, F., Cailleteau, C., Devreux, F., Frugier, P., Gin, S., 2008. Investigation of gel porosity clogging during glass leaching. J. Non-Cryst. Solids 354, 4952–4958.
Jollivet, P., Frugier, P., Parisot, G., Mestre, J.P., Brackx, E., Gin, S., Schumacher, S., 2012a. Effect of clayey groundwater on the dissolution rate of the simulated nuclear waste glass SON68. J. Nucl. Mater. 420, 508–518.
Jollivet, P., Gin, S., Schumacher, S., 2012b. Forward dissolution rate of silicate glasses of nuclear interest in clay-equilibrated groundwater. Chem. Geol. 330–331, 207–217.
Jordan, N., Marmier, N., Lomenech, C., Giffaut, E., Ehrhardt, J.J., 2007. Sorption of silicates on goethite, hematite, and magnetite: experiments and modelling. J. Colloid Interface Sci. 312, 224–229.
Lenting, C., Plümper, O., Kilburn, M., Guagliardo, P., Klinkenberg, M., Geisler, T., 2018. Towards a unifying mechanistic model for silicate glass corrosion. npj Materials Degradation 2, 28.
Mayant, C., Grambow, B., Abdelouas, A., Ribet, S., Ledercq, S., 2008. Surface site density, silicic acid retention and transport properties of compacted magnetite powder. Phys. Chem. Earth 33, 991–999.
McVay, G.L., Buckwalter, C.Q., 1983. Effect of iron on waste-glass leaching. J. Am. Ceram. Soc. 66, 170–174.
Mercado-Depierre, S., Angeli, F., Frizon, F., Gin, S., 2013. Antagonist effects of calcium on borosilicate glass alteration. J. Nucl. Mater. 441, 402–410.
Michelin, A., Burger, E., Leroy, E., Foy, E., Neff, D., Benzerara, K., Dillmann, P., Gin, S., 2013a. Effect of iron metal and siderite on the durability of simulated archeological glassy material. Corros. Sci. 76, 403–414.
Michelin, A., Burger, E., Rebiscoul, D., Neff, D., Bruguier, F., Drouet, E., Dillmann, P., Gin, S., 2013b. Silicate glass alteration enhanced by iron: origin and long-term implications. Environ. Sci. Technol. 47, 750–756.
Michelin, A., Leroy, E., Neff, D., Dynes, J.J., Dillmann, P., Gin, S., 2015. Archeological slag from Glinet: an example of silicate glass altered in an anoxic iron-rich environment. Chem. Geol. 413, 28–43.
Neeway, J., Abdelouas, A., Grambow, B., Schumacher, S., 2011. Dissolution mechanism of the SON68 reference nuclear waste glass: new data in dynamic system in silica saturation conditions. J. Nucl. Mater. 415, 31–37.
Neeway, J.J., Abdelouas, A., Ribet, S., El Mendili, Y., Schumacher, S., Grambow, B., 2015. Effect of Callovo-Oxfordian clay rock on the dissolution rate of the SON68 simulated nuclear waste glass. J. Nucl. Mater. 459, 291–300.
Neff, D., 2003. Contribution of Archaeological Analogs to the Estimation of Average Corrosion Rates and Long Term Corrosion Mechanisms of Low Carbon Steel in Soil. Université de Technologie de Compiègne.
Neff, D., Dillmann, P., Bellot-Gurlet, L., Beranger, G., 2005. Corrosion of iron archaeological artefacts in soil: characterisation of the corrosion system. Corros. Sci. 47, 515–535.
Neill, L., Gin, S., Ducasse, T., De Echave, T., Fournier, M., Jollivet, P., Gourgiotis, A., Wall, N.A., 2017. Various effects of magnetite on international simple glass (ISG) dissolution: implications for the long-term durability of nuclear glasses. npj Materials Degradation 1, 1.
Ngo, D., Liu, H., Sheth, N., Lopez-Hallman, R., Podraza, N.J., Collin, M., Gin, S., Kim, S.H., 2018. Spectroscopic ellipsometry study of thickness and porosity of the alteration layer formed on international simple glass surface in aqueous corrosion conditions. npj Materials Degradation 2, 20.
Odorowski, M., Jegou, C., De Windt, L., Broudic, V., Jouan, G., Peuget, S., Martin, C., 2017. Effect of metallic iron on the oxidative dissolution of UO2 doped with a radioactive alpha emitter in synthetic Callovian-Oxfordian groundwater. Geochem. Cosmochim. Acta 219, 1–21.
Pèlegrin, E., Calas, G., Ildefonse, P., Jollivet, P., Galoisy, L., 2010. Structural evolution of glass surface during alteration: application to nuclear waste glasses. J. Non-Cryst. Solids 356, 2497–2508.
Philippini, V., Naveau, A., Catalette, H., Leclercq, S., 2006. Sorption of silicon on magnetite and other corrosion products of iron. J. Nucl. Mater. 348, 60–69.
Rébiscoul, D., Burger, E., Bruguier, F., Godon, N., Chouchan, J.L., Mestre, J.P., Frugier, P., Lartigue, J.E., Gin, S., 2013. Glass-Iron-Clay interactions in a radioactive waste geological disposal: a multiscale approach. MRS Proceedings 1518, 185–190.
Rebiscoul, D., Frugier, P., Gin, S., Ayral, A., 2005. Protective properties and dissolution ability of the gel formed during nuclear glass alteration. J. Nucl. Mater. 342, 26–34.
Rebiscoul, D., Van der Lee, A., Rieutord, F., Né, F., Spalla, O., El-Mansouri, A., Frugier, P., Ayral, A., Gin, S., 2004. Morphological evolution of alteration layers formed during nuclear glass alteration: new evidence of a gel as a diffusive barrier. J. Nucl. Mater. 326, 9–18.
Rolland, S., Tribet, M., Broudic, V., Jollivet, P., Jégou, C., Toulhoat, P., 2012. Effect of groundwater on the dissolution rate of the simulated nuclear waste glass SON68 under gamma irradiation. Procedia Chemistry 7, 587–592.
Romaine, A., Sabot, R., Jeannin, M., Necib, S., Refait, P., 2013. Electrochemical synthesis and characterization of corrosion products on carbon steel under argillite layers in carbonated media at 80 degrees C. Electrochim. Acta 114, 152–158.
Rull, F., Martinez-Frias, J., Sansano, A., Medina, J., Edwards, H.G.M., 2004. Comparative micro-Raman study of the Nakhla and Vaca Muerta meteorites. J. Raman Spectrosc. 35, 497–503.
Saheb, M., Descostes, M., Neff, D., Matthiesen, H., Michelin, A., Dillmann, P., 2010. Iron corrosion in an anoxic soil: comparison between thermodynamic modelling and ferrous archaeological artefacts characterised along with the local in situ geochemical conditions. Appl. Geochem. 25, 1937–1948.
Schlegel, M.L., Bataillon, C., Brucker, F., Blanc, C., Prêt, D., Foy, E., Chorro, M., 2014. Corrosion of metal iron in contact with anoxic clay at 90 °C: characterization of the corrosion products after two years of interaction. Appl. Geochem. 51, 1–14.
Schlegel, M.L., Martin, C., Brucker, F., Bataillon, C., Blanc, C., Chorro, M., Jollivet, P., 2016. Alteration of nuclear glass in contact with iron and claystone at 90 °C under anoxic conditions: characterization of the alteration products after two years of interaction. Appl. Geochem. 70, 27–42.
Sessegolo, L., Verney-Carron, A., Saheb, M., Remusat, L., Gonzalez-Cano, A., Nuns, N., Mertz, J.-D., Loisel, C., Chabas, A., 2018. Long-term weathering rate of stained-glass windows using H and O isotopes. npj Materials Degradation 2, 17.
Thien, B.M.J., Godon, N., Ballestero, A., Gin, S., Ayral, A., 2012. The dual effect of Mg on the long-term alteration rate of AVM nuclear waste glasses. J. Nucl. Mater. 427, 297–310.
van Aken, P.A., Liebscher, B., Styrsa, V.J., 1998. Quantitative determination of iron oxidation states in minerals using Fe L2,3-edge electron energy-loss near-edge structure spectroscopy. Phys. Chem. Miner. 25, 323–327.
Van Iseghem, P., Aertsens, M., Gin, S., Deneele, D., Grambow, B., Strachan, D., McGrail, P., Wicks, G., 2009. Glamor - or how we achieved a common understanding on the decrease of glass dissolution kinetics. In: Environmental Issues and Waste Management Technologies in the Materials and Nuclear Industries Xii. Amer Ceramic Soc, Westerville, pp. 115–126.
Vienna, J.D., Ryan, J.V., Gin, S., Inagaki, Y., 2013. Current understanding and remaining challenges in modeling long-term degradation of borosilicate nuclear waste glasses. Int. J. Appl. Glass Sci. 4, 283–294.
Wray, J.L., Daniels, F., 1957. PRECIPITATION OF CALCITE AND ARAGONITE. J. Am. Chem. Soc. 79, 2031–2034.